Research Article | Vol. 10, No. 9 / 1 September 2019 / Biomedical Optics Express 4676
Biomedical Optics EXPRESS

Quantifying skin photodamage with spatial frequency domain imaging: statistical results

JEFFREY B. TRAVERS,[1,2,3] CHIEN POON,[4] TREVOR BIHL,[1,4] BENJAMIN RINEHART,[4] CHRISTINA BORCHERS,[1] DANIEL J. ROHRBACH,[4] SAMIA BORCHERS,[2] JULIAN TREVINO,[2] MAX RUBIN,[2] HEIDI DONNELLY,[2] KARL KELLAWAN,[2] LYDIA CARPENTER,[2] SHALINI BAHL,[2] CRAIG ROHAN,[2] ELIZABETH MUENNICH,[2] SCOTT GUENTHNER,[5] HOLLY HAHN,[2] ALI RKEIN,[2] MARC DARST,[6] NICO MOUSDICAS,[7] ELIZABETH CATES,[1] AND ULAS SUNAR[4,*]

[1]*Department of Pharmacology & Toxicology, Boonshoft School of Medicine, Wright State University, Dayton, OH 45435, USA*
[2]*Department of Dermatology, Boonshoft School of Medicine, Wright State University, Dayton, OH 45435, USA*
[3]*Dayton Veterans Administration Medical Center, Dayton, OH 45428, USA*
[4]*Department of Biomedical, Industrial & Human Factors Engineering, Wright State University, Dayton, OH 45435, USA*
[5]*Dermatology Center of Indiana, Plainfield IN 46168, USA*
[6]*Charlotte Dermatology, Charlotte, NC 28277, USA*
[7]*Richard L. Roudebush VA Medical Center, Indianapolis, IN 46202, USA*
[*]*ulas.sunar@wright.edu*

Abstract: We investigated the change in optical properties and vascular parameters to characterize skin tissue from mild photodamage to actinic keratosis (AK) with comparison to a published photodamage scale. Multi-wavelength spatial frequency domain imaging (SFDI) measurements were performed on the dorsal forearms of 55 adult subjects with various amounts of photodamage. Dermatologists rated the levels of photodamage based upon the photographs in blinded fashion to allow comparison with SFDI data. For characterization of statistical data, we used artificial neural networks. Our results indicate that optical and vascular parameters can be used to quantify photodamage and can discriminate between the stages as low, medium, and high grades, with the best performance of ~70%, ~76% and 80% for characterization of low- medium- and high-grade lesions, respectively. Ultimately, clinicians can use this noninvasive approach for risk assessment and frequent monitoring of high-risk populations.

1. Introduction

Ultraviolet (UV) light exposure is the major cause for skin photodamage. UV exposures commonly encountered include sunlight and indoor tanning bed exposure. Pathologic effects of UV radiation include precancerous actinic keratosis (AK), which can progress into basal cell carcinoma (BCC) and squamous cell carcinoma (SCC). Actinic neoplasia (precancerous actinic keratosis and non-melanoma skin cancer) are highly prevalent in elderly patients with fair skin, and those with compromised immune systems. The impact on our healthcare system is substantial, as currently the average annual cost to treat non-melanoma skin cancer is 5 billion dollars [1]. Though often a source of considerable morbidity due to extensive surgical procedures to remove the skin cancers in the normal populations, SCCs are a common source of mortality in immunosuppressed populations, including solid organ transplant recipients. Thus, it is important to predict if patients have actinic neoplasia for prevention and accurate intervention decision

#374903
Journal © 2019
https://doi.org/10.1364/BOE.10.004676
Received 7 Aug 2019; accepted 8 Aug 2019; published 20 Aug 2019

Biomedical Optics EXPRESS

making. Ideally, a non-invasive imaging approach in a clinical setting could be used for frequent monitoring of patients at high risk for actinic neoplasia.

A recent preclinical study has suggested that noninvasive imaging of skin could detect and monitor precancerous lesions using hemoglobin contrast [2]. Similarly, our group has reported a pilot study showing the feasibility that spatial frequency domain imaging (SFDI) could be used to identify skin actinic damage in three patients [3]. SFDI is a wide-field, non-contact mesoscopic optical imaging modality that can provide multiple parameters concurrently [4–6]. In reflectance mode, it can provide maps of optical properties (absorption and scattering) and vascular parameters (hemoglobin concentrations and tissue oxygen saturation) [6–13]. In fluorescence imaging mode, it can utilize high fluorescence contrast and provide absolute drug fluorescence concentration maps that can allow early detections of premalignant lesions [14,15]. Here, we present the results from a statistically valid patient number (N = 55 subjects; 110 dorsal forearms). We investigated the changes in optical properties and vascular parameters derived by SFDI to characterize skin tissue based on photodamage. The results were compared to photodamage scores from dermatologists (N = 15 physicians) trained in evaluating actinic damage.

2. Methods

We performed a clinical study under an institutional review board-approved protocol, and informed consent was obtained from all the patients before the measurements. The study was conducted on subjects who are patients in the Wright State University Department of Dermatology clinics. The patients were 35 years old or older with "fair" skin (Fitzpatrick scale I or II) [16], and did not have recent history of use of a tanning bed/significant sun exposure. There were total 55 subjects expressing various levels of photodamage, including clinically-apparent AKs. Their level of UV skin damage on their bilateral forearms was photographed and categorized by 15 board-certified dermatologists according to Global Assessment Severity Scale ranging from 0 (less severe) to 9 (the most progressed stage of skin damage) using a validated tool [16]. With 55 subjects, both arms were treated as separate images when presented to the dermatologists, yielding 110 images to be analyzed per dermatologist, thus 1,650 dermatologist scores were collected across all samples. The physicians rated each forearm from 0-9, with scores tending towards the middle values (Fig. 1(a)).

In addition to scores being predominantly in the middle range, scores also saw a range in dermatology scores on the same patient/arm combination (Fig. 1(b)). To remove inconsistent results, a control chart approach was applied to the ranges where samples (arm, patient pairs) associated with ranges outside a 95% confidence interval on the overall range mean was applied. This resulted in samples with a range of 5 or above, i.e. one dermatologist rating an arm as a 9 and another as a 4, being removed from the dataset. This resulted in 17 observations (arm, patient combinations), i.e. 255 dermatologist scores, being removed from analysis. The average range in scores changed from 3.57 to 3.25, but the ranges were all within an upper confidence interval on the range.

In McKenzie et al [16]. the scores were further dichotomized into four levels: scores 0 being no actinic damage, scores 1, 2, of 3 being low, scores 4, 5 6 being moderate, and 7, 8, 9 being severe. Consistent with this grouping, the collected ratings were grouped into low (scores $\leq$3), medium (scores $\geq$4 and $\leq$6), and high (scores $\geq$7) levels of photodamage, with representative examples seen Fig. 1(b). In order to estimate the true damage, ensemble approaches were used was to take all $N = 15$ observations for a given arm and rate the arm with a single rating. Four ensemble approaches were considered: minimum of all ratings, maximum of all ratings, median of all ratings, and mode of all ratings; from here the arms were then grouped into the low, medium, and high levels.

Biomedical Optics EXPRESS

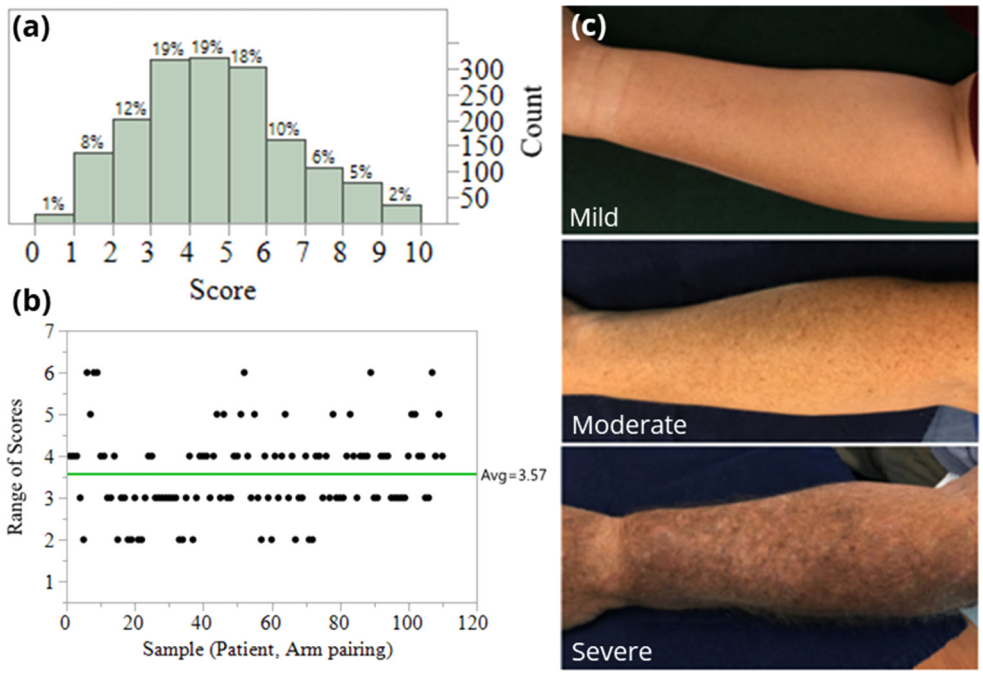

Fig. 1. (a) Dermatologists' clinical scores of skin damage. (b) Range of scores from dermatologists. (c) Examples of mild, moderate, severe photodamage analyzed by clinical dermatologists.

The results are compared with the quantitative maps obtained by the SFDI analysis detailed below. The SFDI analysis generated maps of absorption, scattering, hemoglobin concentrations, and tissue oxygen saturation.

For the SFDI data acquisition, our SFDI instrument was described previously in our pilot study reports [17,18] (Fig. 2). Briefly, light from light emitting diodes (LEDs) with center wavelengths of 490nm, 590nm and 660nm (LCS series, Mightex, Toronto, Ontario, Canada) were focused into a liquid light guide and directed onto a digital micromirror device (DMD) having 1140×912 pixel resolution (DLP LightCrafter 4500, Texas Instruments, Dallas, TX). The LEDs were sequentially selected with a four-channel LED controller (SLC-SA04-US, Mightex, Toronto, Ontario, Canada) so that only one wavelength was on at a time. The DMD generated sine wave patterns with 6 different frequencies ranging from 0 to 0.27 mm-1, with three phases (0, $2\pi/3$, $4\pi/3$) for each frequency. The patterns were projected onto the tissue surface and the reflected image was acquired with a sCMOS camera (Zyla, Andor Technology, Belfast, United Kingdom). Crossed polarizers in front of the camera and DMD rejected any specular reflection. A custom, 3-D printed light shield with an imaging window blocked room light and kept the skin surface at the focal plane of both the DMD and camera. A custom LabView (National Instruments, Austin, TX) program controlled the LED current and camera exposure times.

For the SFDI data analysis, approximate areas of 3 cm x 4cm on the subjects' arm were imaged and analyzed with SFDI technique. For each frequency, the three phases were demodulated to extract the spatially modulated component of the diffuse reflectance [4]. The reflectance data for each wavelength at each pixel were then fitted to a "white Monte Carlo" model to quantify absorption (μ_a) and reduced scattering (μ_s') of each lesion [4]. Tissue scattering was modeled as Mie type behavior, $\mu_s' = A(\lambda/\lambda_0)^{-B}$, where λ_0 is the normalization wavelength (700 nm), the parameter A characterizes the magnitude of scattering and B characterizes the wavelength

Biomedical Optics EXPRESS

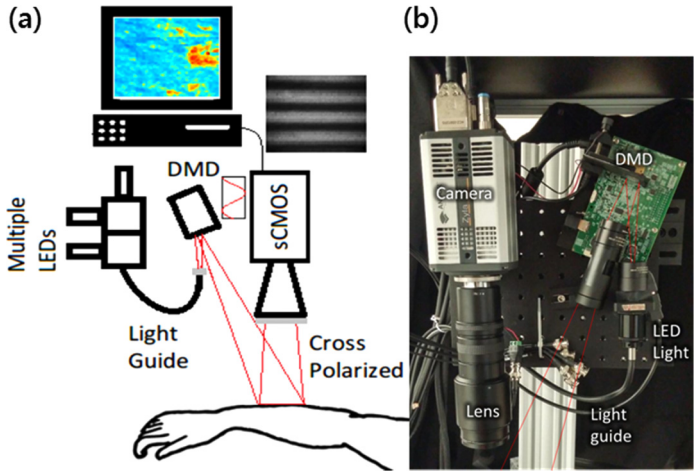

Fig. 2. (a) Schematic diagram and (b) photo of SFDI instrument for imaging lesions on arm.

dependence, related to scattering power [19]. Both A and B were determined using a nonlinear algorithm (lsqnonlin, Matlab) to fit the scattering at each pixel to the Mie model. To obtain the hemoglobin parameters, the absorption parameter was modeled as a linear combination of the primary tissue absorbers, $\mu_a = C_{oxy}\mu^{oxy} + C_{deoxy}\mu^{deoxy} + C_{mel}\mu^{mel} + \mu_a^{back}$. Here μ and C represent the absorption coefficient and concentration of each component (HbO_2, Hb and melanin) respectively, and $\mu_a{}^{back}$ is assumed to be fixed background absorption coefficient originated from water. We fitted for melanin with the assumption of the power law following Jacques [20]. The total hemoglobin concentration (THC) and the blood oxygenation saturation (StO_2) maps were calculated from the quantified Coxy (HbO_2) and Cdeoxy (Hb), as THC = Coxy + Cdeoxy, and StO_2=Coxy/THC. Due to the highly nonlinear nature of the data, these parameters were fed into the artificial neural network (ANN) analysis for group classification with respect to each parameter. The ANN was constructed using a 3-layer feedforward architecture with 24 log-sigmoidal hidden nodes, consistent with previous work [21,22]. Scaled conjugate gradient was used to train the ANN with 1000 training iteration and a goal of 0.001 mean squared error (MSE). For training the ANN, the data was split into training/testing and validation sets. The training/testing set was used for ANN model generation and the validation set was sequestered and used to evaluate the final performance of the ANN algorithm. The model development data was randomly allocated into three groups: 60% for training, 20% for testing, and 20% sequestered for validation.

3. Results and discussion

Figure 3 shows representative reconstructed images of optical absorption from three patients having different scale of actinic damage. Representative SFDI quantitative images of absorption parameter at 490nm for 3 patients are shown in Fig. 3(a), (b), and (c), respectively. Patient 3 had 166% higher absorption than patient 1 ($5.13 \pm 2.15 cm^{-1}$ vs. $1.93 \pm 0.34\ cm^{-1}$). In addition, the percent variation for absorption across each image (standard deviation divided by mean, a measure of tissue heterogeneity) was lower for patient 1 and 2 than for patient 3 (17.6%, 27.5% and 41.9%), highlighting the increased heterogeneity for patients 3 due to increasing sun damage score. Thus, these results indicate there exist differences in the absorption parameter distributions in these patients.

After obtaining images for each parameter, their mean, std were calculated. The Dermatologists' scores had variance both with the internal controls and also with each other's assessments. This

Biomedical Optics EXPRESS

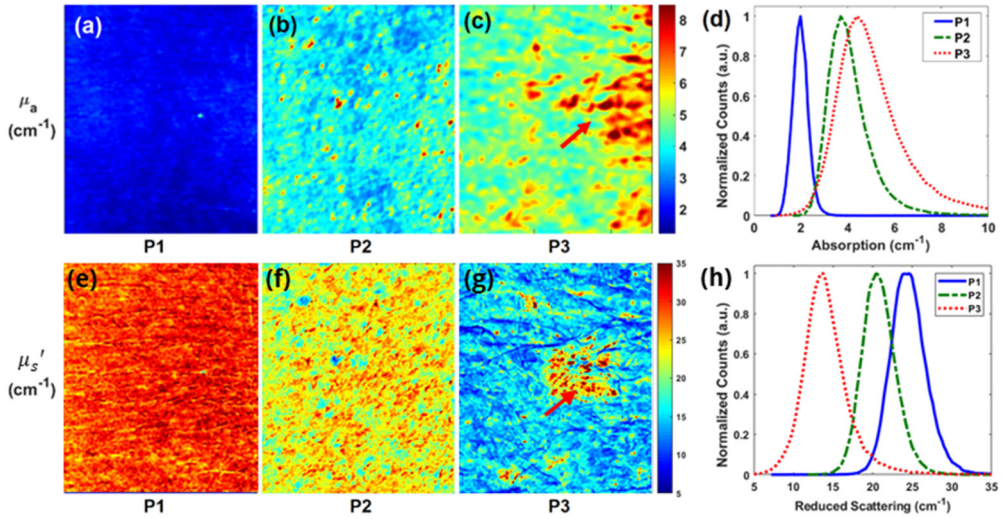

Fig. 3. (a), (b), (c) Absorption imaging maps and the (e), (f), (g) reduced scattering maps for three subjects at 490 nm. Red arrows highlight the visible lesion for subject with severe photodamage (P3). (d) Histograms of the absorption parameter and the (h) reduced scattering parameter for the subjects with mild (P1), moderate (P2), and severe damage (P3) at 490 nm.

reduction in the grading system resulted in possible classification with high accuracy since the 10-level scale provided only sparse sampling at the low and high ends. Figure 4 shows differences between groups of low (scores <4), medium (scores >3 and <7), and high (scores >6) levels of photodamage with respect to (a) scattering power, B (b) total hemoglobin concentration, THC (c) deoxy-hemoglobin concentration, C_{deoxy}.

Table 1 shows the ANN classification with respect to the variables A_mean, A_std, b_mean, b_std, Coxy_mean, Coxy_std, Cdeoxy_mean, Cdeoxy_std, THC_mean, THC_std, Mel_mean, and Mel_std. Notably, this includes the parameters identified in Fig. 4, (a) scattering power, B (b) total hemoglobin concentration, THC (c) deoxy-hemoglobin concentration, C_{deoxy}, which had the ability to characterize these reduced 3 clinical scores of the skin damage. We chose to show only these 3 parameters in Fig. 4 because they have high characterization power, which aligns well with our previous publication [3], and being independent from each other in physiological context: B is related to tissue scattering parameter, related to cell structure, THC is related to blood volume or microvasculature formation, C_{deoxy} is related to oxygen consumption or metabolism. Table 1 presents classification results for the ANN using each of the 4 ensemble methods. Overall, the ANN when using ensembles via the minimum of scores approach is able to classify SFDI scores into the three (low, medium, high) groups at a rate much better than chance. Median, Mode, and Maximum ensemble approaches were found to be inaccurate, overall or to one or more groupings. This is true both in the model building results, Training/Testing, and in the prediction results seen in the validation column. Furthermore, the ANN was always accurate when detecting the high damage group.

As for the limitations in this study, only three wavelengths were used for multiwavelength fitting due to availability of the light sources in our instrument. We acknowledge that the use of fewer wavelengths may lead to less stable fitting, resulting in reduced accuracy in the quantified parameters. Adding more wavelengths may allow more accurate quantification and thereby better contrasts. Melanin in particular can be a difficult absorber to quantify due to its featureless absorption spectrum and uneven distribution in the skin [18,23]. Future study plans include adding more LEDs at different wavelengths in the range of [450nm-700nm].

Biomedical Optics EXPRESS

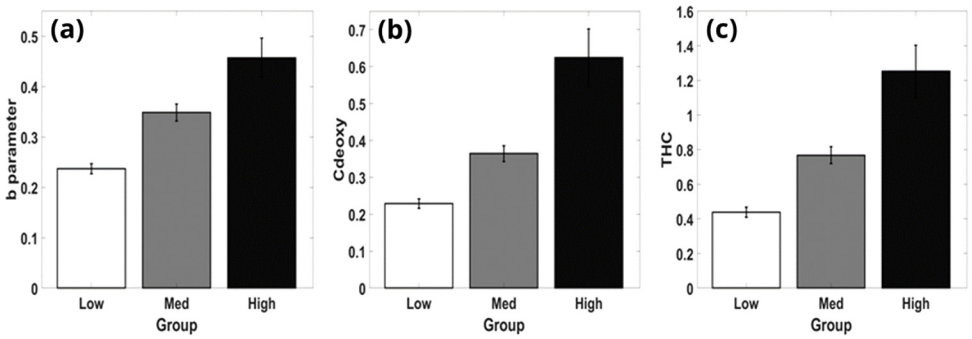

Fig. 4. Separation of groups possible with respect to (a) scattering power, B (b) deoxy-hemoglobin concentration, C_{deoxy} (c) total hemoglobin concentration, THC.

Table 1. Classification accuracy results for ANN by group.

		Training	Testing	Validation – sequestered data with S.E. interval
Min (best performance)	Low	81.2%	77.8%	70.3%±0.4%
	Medium	73.3%	66.7%	76.3%±9.6%
	High	100%	100%	80%±13.3%
Median	Low	63.5%	63%	53.8%±1.1%
	Medium	61.7%	60%	60.5%±0.8%
	High	100%	0%	80%±13.3%
Max	Low	0%	0%	0%±0%
	Medium	62.2%	63.2%	61.4%±1.2%
	High	66.2%	66.7%	81.6%±2.5%
Mode	Low	61.9%	58.3%	51.7%±1.9%
	Medium	56.5%	84.6%	60.4%±1.2%
	High	0%	0%	50%±16.7%

There are also potential limitations in both acquisition and analysis speed. SFDI images were obtained via post-processing with custom MATLAB software that fit the data to the model at each pixel. This post-processing took between 5 and 10 minutes depending on the pixel binning and was performed outside the clinic. In total, the data acquisition time in the clinic was around 1 minute, and pixel by pixel fitting for optical properties took 1-2 minute per wavelength and the multi-wavelength fitting took 2-3 minutes. These times could be reduced by binning for fewer pixels, but a better approach would be utilizing a faster acquisition technique such as single snapshot [24] and a faster processing technique such as the look up table (LUT) model recently proposed [25], which could reduce the overall quantification time and provide results in the clinic. This near real-time feedback would be particularly useful for monitoring light-based therapies such as laser or photodynamic therapy. We expect that this non-invasive technology could be used to not only assess skin for risk for actinic neoplasia, but also as a tool to be able to study field carcinogenesis [26]. Although the imaging is not at the stage of replacing any clinical practice, it can provide beneficial feedback to guide clinicians and improve the sensitivity, specificity and speed of the characterization of the lesions. Thus, in the long-term it can induce impact, at least with respect to reducing the financial burden.

Biomedical Optics EXPRESS

4. Conclusion

This clinical study indicates that SFDI can provide quantitative maps of optical and vascular parameters of precancerous lesions such as AK in a statistically valid population, N = 55, and that there is a trend with optical and vascular parameters with respect to levels of photodamage. SFDI parameters could be correlated well with the clinical grading as long as lesion stages can be reduced to three as being low, medium and high. The accuracy of staging was lower for the larger level groupings. Thus, SFDI can be used for assessing three-level staging. Since it is noninvasive and uses a noncontact technique, it can provide additional feedback regarding changes in the stages of pre-cancerous lesion by frequent monitoring of patients.

Funding

Ohio Third Frontier to the Ohio Imaging Research and Innovation Network (OIRAIN) (667750); National Institutes of Health (100000002) (AG048946, ES020866, HL062996); Veteran's Administration Merit Awards (1101CX000809, 5I01BX000853).

Disclosures

The authors declare that there are no conflicts of interest related to this article.

References

1. H. W. Rogers, M. A. Weinstock, S. R. Feldman, and B. M. Coldiron, "Incidence Estimate of Nonmelanoma Skin Cancer (Keratinocyte Carcinomas) in the U.S. Population, 2012," JAMA Dermatol. **151**(10), 1081–1086 (2015).
2. R. L. Konger, Z. Xu, R. P. Sahu, B. M. Rashid, S. R. Mehta, D. R. Mohamed, S. C. DaSilva-Arnold, J. R. Bradish, S. J. Warren, and Y. L. Kim, "Spatiotemporal assessments of dermal hyperemia enable accurate prediction of experimental cutaneous carcinogenesis as well as chemopreventive activity," Cancer Res. **73**(1), 150–159 (2013).
3. J. B. Travers, C. Poon, D. J. Rohrbach, N. M. Weir, E. Cates, F. Hager, and U. Sunar, "Noninvasive mesoscopic imaging of actinic skin damage using spatial frequency domain imaging," Biomed. Opt. Express **8**(6), 3045–3052 (2017).
4. D. J. Cuccia, F. Bevilacqua, A. J. Durkin, F. R. Ayers, and B. J. Tromberg, "Quantitation and mapping of tissue optical properties using modulated imaging," J. Biomed. Opt. **14**(2), 024012 (2009).
5. D. J. Cuccia, F. Bevilacqua, A. J. Durkin, and B. J. Tromberg, "Modulated imaging: quantitative analysis and tomography of turbid media in the spatial-frequency domain," Opt. Lett. **30**(11), 1354–1356 (2005).
6. J. P. Angelo, S. J. Chen, M. Ochoa, U. Sunar, S. Gioux, and X. Intes, "Review of structured light in diffuse optical imaging," J. Biomed. Opt. **24**(07), 1–20 (2018).
7. R. B. Saager, D. J. Cuccia, S. Saggese, K. M. Kelly, and A. J. Durkin, "A light emitting diode (LED) based spatial frequency domain imaging system for optimization of photodynamic therapy of nonmelanoma skin cancer: quantitative reflectance imaging," Lasers Surg. Med. **45**(4), 207–215 (2013).
8. R. B. Saager, D. J. Cuccia, and A. J. Durkin, "Determination of optical properties of turbid media spanning visible and near-infrared regimes via spatially modulated quantitative spectroscopy," J. Biomed. Opt. **15**(1), 017012 (2010).
9. X. Chen, W. Lin, C. Wang, S. Chen, J. Sheng, B. Zeng, and M. Xu, "In vivo real-time imaging of cutaneous hemoglobin concentration, oxygen saturation, scattering properties, melanin content, and epidermal thickness with visible spatially modulated light," Biomed. Opt. Express **8**(12), 5468–5482 (2017).
10. A. Yafi, F. K. Muakkassa, T. Pasupneti, J. Fulton, D. J. Cuccia, A. Mazhar, K. N. Blasiole, and E. N. Mostow, "Quantitative skin assessment using spatial frequency domain imaging (SFDI) in patients with or at high risk for pressure ulcers," Lasers Surg. Med. **49**(9), 827–834 (2017).
11. B. Yang, J. Lesicko, A. Moy, J. Reichenberg, M. Sacks, and J. W. Tunnell, "Color structured light imaging of skin," J. Biomed. Opt. **21**(5), 050503 (2016).
12. S. Nandy, I. S. Hagemann, M. A. Powell, C. Siegel, and Q. Zhu, "Quantitative multispectral ex vivo optical evaluation of human ovarian tissue using spatial frequency domain imaging," Biomed. Opt. Express **9**(5), 2451–2456 (2018).
13. A. M. Laughney, V. Krishnaswamy, E. J. Rizzo, M. C. Schwab, R. J. Barth Jr., D. J. Cuccia, B. J. Tromberg, K. D. Paulsen, B. W. Pogue, and W. A. Wells, "Spectral discrimination of breast pathologies in situ using spatial frequency domain imaging," Breast Cancer Res. **15**(4), R61 (2013).
14. R. B. Saager, D. J. Cuccia, S. Saggese, K. M. Kelly, and A. J. Durkin, "Quantitative fluorescence imaging of protoporphyrin IX through determination of tissue optical properties in the spatial frequency domain," J. Biomed. Opt. **16**(12), 126013 (2011).
15. U. Sunar, D. J. Rohrbach, J. Morgan, N. Zeitouni, and B. W. Henderson, "Quantification of PpIX concentration in basal cell carcinoma and squamous cell carcinoma models using spatial frequency domain imaging," Biomed. Opt. Express **4**(4), 531–537 (2013).

Biomedical Optics EXPRESS

16. N. E. McKenzie, K. Saboda, L. D. Duckett, R. Goldman, C. Hu, and C. N. Curiel-Lewandrowski, "Development of a photographic scale for consistency and guidance in dermatologic assessment of forearm sun damage," Arch. Dermatol. **147**(1), 31–36 (2011).
17. D. J. Rohrbach, D. Muffoletto, J. Huihui, R. Saager, K. Keymel, A. Paquette, J. Morgan, N. Zeitouni, and U. Sunar, "Preoperative mapping of nonmelanoma skin cancer using spatial frequency domain and ultrasound imaging," Acad. Radiol. **21**(2), 263–270 (2014).
18. D. J. Rohrbach, N. C. Zeitouni, D. Muffoletto, R. Saager, B. J. Tromberg, and U. Sunar, "Characterization of nonmelanoma skin cancer for light therapy using spatial frequency domain imaging," Biomed. Opt. Express **6**(5), 1761–1766 (2015).
19. J. R. Mourant, T. Fuselier, J. Boyer, T. M. Johnson, and I. J. Bigio, "Predictions and measurements of scattering and absorption over broad wavelength ranges in tissue phantoms," Appl. Opt. **36**(4), 949–957 (1997).
20. S. L. Jacques and D. J. McAuliffe, "The melanosome: threshold temperature for explosive vaporization and internal absorption coefficient during pulsed laser irradiation," Photochem. Photobiol. **53**(6), 769–775 (1991).
21. T. J. Bihl, W. A. Young II, and G. R. Weckman, "Artificial Neural Networks and Their Applications in Business," in *Encyclopedia of Information Science and Technology*, 4 ed. (2018), pp. 6642–6657.
22. R. O. Duda, P. E. Hart, and D. G. Stork, *Pattern Classification* (John Wiley & Sons, 2012).
23. R. B. Saager, A. Sharif, K. M. Kelly, and A. J. Durkin, "In vivo isolation of the effects of melanin from underlying hemodynamics across skin types using spatial frequency domain spectroscopy," J. Biomed. Opt. **21**(5), 057001 (2016).
24. M. van de Giessen, J. P. Angelo, and S. Gioux, "Real-time, profile-corrected single snapshot imaging of optical properties," Biomed. Opt. Express **6**(10), 4051–4062 (2015).
25. J. Angelo, C. R. Vargas, B. T. Lee, I. J. Bigio, and S. Gioux, "Ultrafast optical property map generation using lookup tables," J. Biomed. Opt. **21**(11), 110501 (2016).
26. M. G. Kemp, D. F. Spandau, and J. B. Travers, "Impact of Age and Insulin-Like Growth Factor-1 on DNA Damage Responses in UV-Irradiated Human Skin," Molecules **22**(3), 356 (2017).